Journal of The Electrochemical Society, **151** (1) B1-B10 (2004)
0013-4651/2003/151(1)/B1/10/$7.00 © The Electrochemical Society, Inc.

Characterization of Oxide Films Formed on Mg-Based WE43 Alloy Using AC/DC Anodization in Silicate Solutions

V. Birss,[a,*,z] S. Xia,[a] R. Yue,[a] and Richard G. Rateick, Jr.[b]

[a]*Department of Chemistry, The University of Calgary, Calgary, Alberta, Canada T2N 1N4*
[b]*Honeywell Engines Systems and Services, South Bend, Indiana 46620, USA*

The characteristics of the oxide film formed on a Mg-based WE43 alloy using ac/dc anodization techniques in an alkaline silicate solution have been investigated using scanning electron microscopy and Rutherford back-scattering spectroscopy, and the corrosion resistance of these films has been determined using the ac impedance technique. The oxide film was found to be composed of MgO, $Mg(OH)_2$, MgF_2, and SiO_2, and consisted of an inner barrier and an outer porous oxide film, both of which increased linearly in thickness with the applied anodization voltage. High applied voltages and current densities also led to the formation of large pores, having diameters greater than 6 μm, and the partial sealing of small pores in the outer layer. Allowing the current to decay for a period of time in the later stages of anodization led to an increase in the thickness of both the barrier and porous films and further sealing of the film pores. A correlation of the oxide corrosion resistance with the barrier film thickness is also demonstrated.
 [DOI: 10.1149/1.1629095]

Manuscript submitted April 10, 2003; revised manuscript received July 2, 2003. Available electronically November 18, 2003.

Mg alloys have many unique properties compared with other metals. Their most attractive feature is their low density, 1.73 g/cm^3 for pure Mg[1] and approximately 1.80 g/cm^3 for most Mg alloys,[2] about two-thirds that of Al and its alloys. Some other advantages are their very high strength-to-weight ratio, high stiffness, and mechanical castability. In addition, Mg is very abundant, being present in high concentrations in seawater, and it is therefore a comparatively low cost material.

Due to their attractive features, Mg alloys have been used extensively for a wide variety of structural and nonstructural purposes. In order to meet the increasing aerospace demand for lightweight materials with high strength, high performance, and especially high corrosion resistance, strenuous efforts have been directed toward the development of advanced Mg alloys in the last decade. Two new generations of Mg alloys have been identified, having corrosion rates comparable to those of Al-based alloys. One is a high purity Mg-Al alloy, such as AZ91, in which the Fe, Ni, and Cu contents are restricted to less than 50, 50, and 700 ppm, respectively, and a very high corrosion resistance has been achieved. The second type of new alloy is the Mg-Y-Nd-Zr system, with examples being WE54 and WE43. This group of alloys not only benefits from high purity and a lack of microporosity, due to the presence of Zr, but it also shows superior corrosion resistance and can be utilized at elevated temperatures. Therefore, these alloys have become very attractive for aerospace applications, such as in engine components, transmission systems, and helicopter gearboxes operating at temperatures up to 250°C.[3,4]

WE43, developed by Magnesium Elektron Ltd.,[5] is an alloy with high purity, intrinsically high corrosion resistance, and high strength, and long term stability up to 250°C. The chemical composition of WE43A-T6 is given in Table I where T6 denotes the fact that the alloy has been solution treated and artificially aged.[6] The impurities in this alloy, particularly Fe, Ni, and Cu, have been reduced to a very low level. Many industrial organizations and research institutes[4,7-9] are actively evaluating and investigating the properties of WE43 in various environments for applications in aerospace, automotive, power tools, recreational equipment, and computers.

Although the WE43 alloy exhibits a relatively high corrosion resistance, it still needs further protection prior to its use in most practical applications. A number of anodic and chemical conversion coating techniques have been developed and are commercially available for Mg alloys,[10-13] relying on the generation of sparks on the alloy surface to develop ceramic-like films. However, some of these processes involve a chromate-based component that is now being restricted by environment regulations. Therefore, the development of chromate-free methods[12-18] is becoming increasingly important. The resultant films formed in these two processes, typically up to tens of micrometers in thickness, are porous, and sealing is often necessary to impart high corrosion resistance to the alloy substrate. For example, our recent work[19] has shown that excellent corrosion resistance can be achieved by sealing with Parylene film.

In one nonchromate process,[12] hydrofluoric acid, which can react with the Mg alloy to form a protective layer of MgF_2 which strongly adheres to the substrate metal and resists further attack, is employed in the bath, along with phosphoric acid and boric acid. However, that process involves the use of a highly toxic and corrosive material, hydrofluoric acid. An alternative anodization process, which is carried out in alkaline solutions with the addition of fluoride ions and aluminate, phosphate, or silicate, has also been developed.[13-18] During anodization, sparks result from the application of a very high voltage, in the range of *ca.* 200 to 400 V, to the Mg alloy. This spark process produces an anodic film containing Mg oxide/hydroxide and other inorganic oxides and compounds. These surface films provide both good corrosion protection and abrasion resistance, as well as offer an excellent paint base for further treatment. When the anodic films are treated further by, for example, sealing and/or painting, an even greater corrosion and abrasion resistance can be expected.

Studies of anodic films formed on magnesium and its alloys in alkaline silicate media are rare,[13,14] compared with those involving alkaline phosphate[15-18] and aluminate[14-16] electrolytes. The present study provides a detailed characterization of anodic films formed on the WE43 alloy in an alkaline silicate electrolyte. The employment of WE43 in this study is specifically for its potential use in aerospace applications. A range of anodizing conditions has been employed in an attempt to determine the optimum film properties by correlating the film morphology with its corrosion resistance. Scanning electron microscopy (SEM) has been employed to examine the morphology and thickness of the oxide films formed at the WE43 alloy, while the Rutherford backscattering (RBS) technique has been employed to establish its composition.

Experimental

WE43 samples.—The magnesium alloy, WE43, was supplied by Magnesium Elektron Ltd. and was cast by Chicago Magnesium under contract from Honeywell International (formerly AlliedSignal Inc.) The composition of the alloy is given in Table I. The working electrode consisted of a disk, 10 mm in diam and 5 mm thick, cut from the ingot. Both faces and the sides were single point machined and then mechanically polished using abrasive emery paper, which gave a surface finish of 0.69 μm R_a. A threaded hole (2 mm diam)

* Electrochemical Society Active Member.
z E-mail: birss@ucalgary.ca

Table I. Composition of WE43-T6 Mg alloy (wt %).[5]

	Y	Nd	Zr	RE[a]	Zn	Li	Mn	Cu	Fe	Si	Ni
Min	3.70	2.00	0.40	0.00	0.00	0.00	0.00	0.00	0.00	0.00	0.00
Max	4.30	2.50	1.00	1.90	0.20	0.20	0.15	0.03	0.01	0.01	0.01
WE43[b]	3.73	2.41	0.53	1.1	0.032	0.125	0.018	0.001	0.003	9×10^{-4}	1×10^{-4}

[a] RE represents other rare earth elements except Nd.
[b] The WE43 was used in this work.

in the side of the disc was designed to fit a stainless steel (SS) rod, used as an electrical contact and to suspend the disc in solution.

WE43 anodization.—Prior to formation of the oxide film, the WE43 disc electrodes were degreased ultrasonically in ethanol for 5 min and then in a mild alkaline solution (0.2 M $Na_2P_2O_7$ + 0.1 M Na_3BO_3 + 0.02 M NaF, pH 10.5) at 70°C for 5 min.[12,13] That alkaline solution, commonly used to brighten die cast alloys, led to an insignificant metal loss after a 5 min treatment. The Teflon-wrapped SS rod holder was then screwed into the disc electrode. After the disc electrode was coated anodically on its side and both faces, this was sometimes followed by a post-treatment and the samples were then left in air for a week or more.

Anodization of the WE43 disks was performed in a 300 mL volume glass cell, having a removable top containing three inlets (for the anode, cathode and a thermometer, placed about 1.5 cm from the anode). The cathode (counter electrode, CE) was a 10 cm^2 316 SS sheet and was located near the base of the cell. The cell was placed in a crystallization dish (2 L vol), used to hold the ice water bath required to maintain the cell solution temperature between 10 and 20°C during the anodizing step. The electrolyte employed to anodize the WE43 alloy was composed of 5-7 g/L KOH, 8-10 g/L KF, and 15-20 g/L Na_4SiO_4, with the final solution pH being 12.5-13.[20] The anodization process was accomplished using a relatively high voltage rectifier which supplied a combination of ac (60 Hz sine wave) and dc power to the electrochemical cell. Typical dc voltages were in the range of 190 to 350 V, and the superimposed ac voltage (root-mean-square, rms value) was maintained at ~20% of the dc.[21] The anodization current densities and voltages, reported in the present paper, represent the sum of the dc and ac components.

Figure 1 shows the two anodization waveforms employed in this work.[22] In both cases, a minimum dc voltage, V_0, of 190 V was initially applied to the anode by the rectifier, causing the current density to spike initially to 50-60 mA/cm^2 (i_0), decaying over 10 to 30 s to the desired current (i_1). After that, the ac voltage was increased from 0 to 38 V, while the dc voltage was kept constant at 190 V. The anodization voltage (sum of dc and ac voltage, maintained at ~20% of dc) was then increased with time from 228 V through V_1 to a final voltage, V_2, using one of two approaches shown in Fig. 1. In waveform A (Fig. 1a), the desired constant current density (i_1) was maintained for a period of time t_1, followed by a period of time ($t_2 - t_1$) of decreasing current to produce an oxide film of a particular thickness. In waveform B (Fig. 1b), the current density, i_1, was kept constant throughout the anodization process by gradually increasing the voltage from V_0 to V_2 at a ramp rate determined by the magnitude of i_1 (V_2 is reached more quickly at higher current densities). The code used to indicate the anodization conditions of waveform A and B is "i_1 for t_1, Δt" ($\Delta t = t_2 - t_1$) and "i_1 for t_2," respectively, where the meaning of i_1, t_1, and t_2 is the same as described above and shown in Fig. 1.

The waveforms shown in Fig. 1 are different from those employed by others in the literature.[15-17] In Ref. 15 and 16, the voltage was increased gradually from 0 V to as high as 330 V at constant current, while in Ref. 17, anodization was carried out at constant

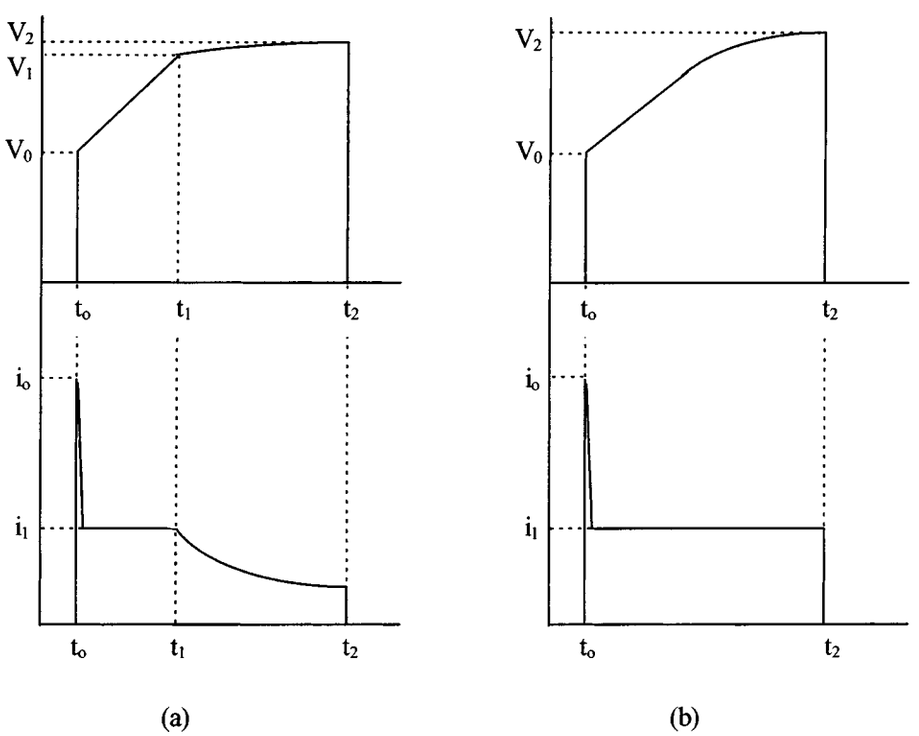

Figure 1. Waveforms employed in WE43 alloy anodization. (a) Type A waveform, (b) type B waveform. $V_0 = 190$ V.

voltage at all times. In contrast, our waveform involved the initial application of 190 V, causing very high currents to flow for a few seconds. Also, waveform A involved a current decay period prior to terminating the anodization, shown below to yield additional benefits to the oxide film corrosion resistance.

Electrochemical measurements.—The impedance measurements were carried out at the open circuit potential (OCP) in 0.86 M NaCl solution using a Solartron 1255 frequency response analyzer connected to a Solartron 1286 electrochemical interface. In this work, the frequencies ranged from 100 kHz to 0.1 Hz, 12 points per decade, with a polarization amplitude of 10 mV (rms). Impedance measurements and data acquisition were achieved using Zplot software. Prior to immersion in the NaCl solution, the sides and one face of the anodized WE43 disc were wrapped with Teflon tape and then coated with epoxy resin, so that only one face (*ca.* 0.78 cm^2) was exposed to solution during corrosion testing.

A saturated calomel electrode (SCE) was used as the reference electrode (RE) in all of this work and a large area platinum gauze electrode was used as the CE for the ac impedance experiments. All solutions used in this work were prepared from analytical grade reagents and triply distilled water (obtained using a Corning MP6A Mega-Pure distillation system). No attempt was made to deaerate the NaCl solution during the impedance measurements.

Surface analysis of oxide films.—The morphology of the oxide films formed at the WE43 alloy was examined with a JSM 6300 V (JEOL) scanning electron microscope, equipped with energy dispersive X-ray analysis (EDX) capabilities. For the cross-sectional analyses, the coated WE43 disc samples were diamond saw cut and mounted in epoxy, filled with glass reinforcement to ensure edge retention during grinding and polishing. The specimens were then ground and polished using standard metallographic techniques, and the film thickness was then determined by SEM analysis of the cross section. Films were also analyzed by RBS using a 2.275 MeV He^{2+} ion beam. The RBS spectra were acquired at a back-scattering angle of 160° and were fit by applying a theoretical model and iteratively adjusting the elemental concentrations until good agreement was found between the theoretical curve and the experimental spectra.

Results and Discussion

General observations during ac/dc anodization of WE43 anodes.—Figure 2 shows the development of the anodization voltage (sum of the ac and dc voltages) as a function of time of anodization of a WE43 sample at an initial current density of 30 mA/cm^2, using both waveforms A and B. In Fig. 2, two different stages in the voltage/time responses can be seen. In the first 5 min, the voltage increased rapidly, indicating the rapid growth of a passivating oxide film on the alloy surface. In that growth stage, sparks which were small and quickly extinguished were seen uniformly distributed on the surface. After 7 min of anodization, the voltage increased much more slowly and almost linearly at the still constant current of 30 mA/cm^2. During this phase, larger and longer-lasting sparks were seen in particular locations on the surface. Large sparks were generally found to be detrimental, reducing the anodization efficiency and the growth rate of the oxide film (see the section on Morphology of anodic oxide films formed on WE43 by ac/dc anodizing, below). After 10 min, the rate of voltage increase for the type A waveform was slightly slower than for type B, as the current had been allowed to decay to below 30 mA/cm^2 in the former case.

The spark frequency and size depended on the anodization current density, with smaller currents yielding fewer and smaller sparks, and when the current density was less than 1 mA/cm^2, almost no sparks were seen. Consistent with this, as the voltage was increased to maintain a constant high current density, even at long times (waveform B), the observed sparks were more frequent and larger. The sparks seen during anodization are the result of the dielectric breakdown of an oxide film. It is believed that further film growth occurred through sites at which the barrier oxide layer had broken down,[17,23] causing visible sparks or scintillation on the anode substrate.

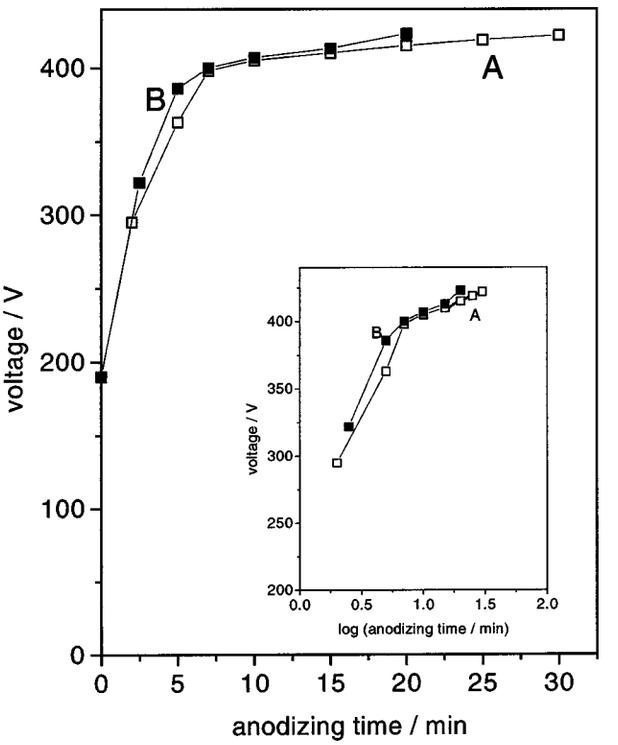

Figure 2. Measured total voltage *vs.* time relationship during anodization of the WE43 alloy at 30 mA/cm^2 using (solid squares) waveform B for 20 min and (open squares) waveform A for 10,20 min in alkaline silicate solution.

Morphology of anodic oxide films formed on WE43 by ac/dc anodizing.—Prior to anodization, a WE43 plate specimen was etched in a 2% Nital solution and its microstructure was determined by optical metallography. Figure 3 shows images of both the longitudinal and transverse plane of the specimen. No dendritic structures were observed. The microstructure was remarkably equiaxed, especially for a cast and solution heat-treated alloy. The size of most of the grains seen in Fig. 3 is 65 μm or finer, while a few grains are as large as 125 μm.

A typical SEM top view image of an oxide film formed on the WE43 alloy is shown in Fig. 4a. The film was deposited using the type A waveform at an initial current density of 30 mA/cm^2 for 5 min, followed by 5 min of decay (30 mA/cm^2 for 5, 5 min) and the final anodization voltage was 385 V. Its cross-sectional image is shown in Fig. 4b. As shown in Fig. 4 and similar to what has been reported previously,[13] the outer part of the oxide film contained pores of diameters in the range of 0.4 to 3.6 μm, with separations between pores of up to *ca.* 5 μm, and a surface porosity of *ca.* 25%. Figure 4b also shows the presence of an intact barrier film beneath the outer porous film.

The dc anodization of Al in acidic solutions (voltage usually about 20 V) involves the dissolution of the oxide, resulting in a film containing a regular distribution of pores, having a diameter and spacing which reliably depends on the applied potential and the anodizing solution.[24,25] However, for the high ac/dc voltage formation of the oxide film at the WE43 alloy in the alkaline silicate medium, the pores seen in Fig. 4 were randomly distributed in the film and many of them appeared to be blocked internally (Fig. 4b). It is therefore likely that the growth mechanism of Mg oxide is different from that of Al oxide under these very different conditions. In the ac/dc anodization of WE43, the intense sparking caused by

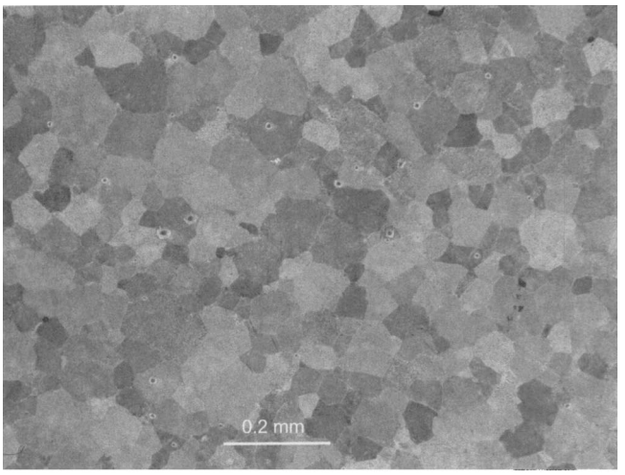

(a)

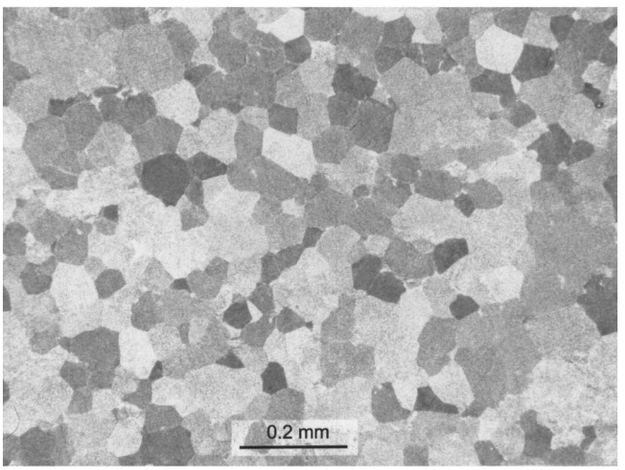

(b)

Figure 3. Microstructure of WE43 specimen in the (a) longitudinal plane and (b) transverse plane of a region at the center of a specimen.

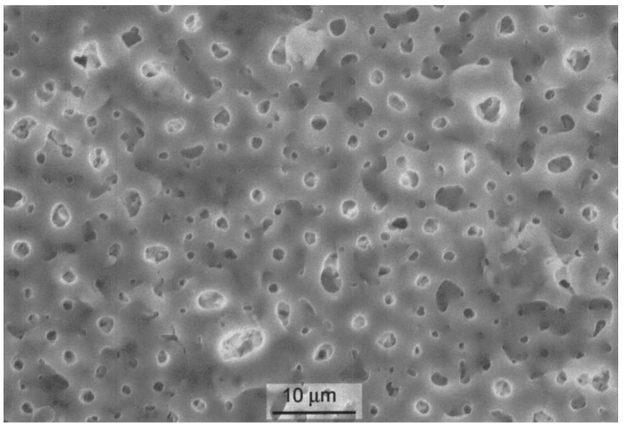

(a)

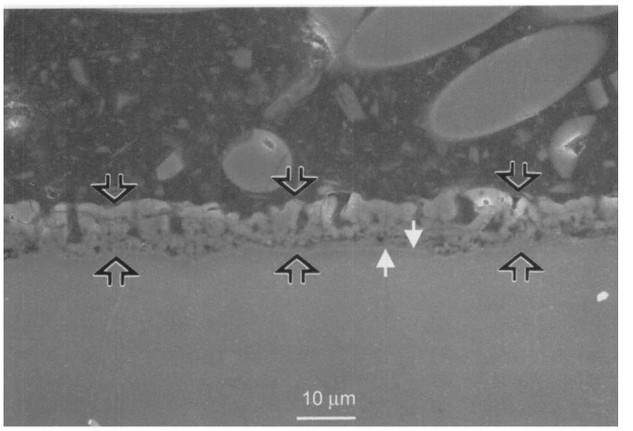

(b)

Figure 4. SEM images of (a) the surface and (b) cross section of WE43 alloy anodized at 30 mA/cm^2 for 5, 5 min in alkaline silicate bath. Barrier layer is between white arrows.

the dielectric breakdown of the film resulted in the formation of thick deposits which resembled sintered ceramic materials.

A closer look at the cross-sectional images in Fig. 4b revealed that this particular oxide film was actually composed of three layers, two outer porous layers, and an inner barrier layer. The outermost layer appeared to have larger pores than the intermediate layer and, while the pores in the outer layer traversed through to the middle layer, they did not penetrate the inner barrier film. Unlike the pores in the outer layer, the pores in the intermediate layer were randomly distributed and somewhat interconnected. The formation of the outer layer likely occurred by oxide fusion at the high temperatures achieved at high voltages, thus reducing the total number of pores, but creating larger pores which were vertical to the substrate. The barrier layer was likely the most significant portion of the film leading to its corrosion resistance, and it is very important to note that the barrier film did not appear to be porous or cracked. The total film thickness in Fig. 4b was 8-12 μm, while the inner barrier film was *ca.* 0.9 μm thick.

In another experiment using waveform A, t_1 (see Fig. 1) was extended to 7 min at 30 mA/cm^2 and the current was then allowed to decay for another 13 min (30 mA/cm^2 for 7, 13 min), reaching a maximum voltage of 408 V. A top view of that oxide film, formed on a freshly polished WE43 specimen, is shown in Fig. 5. Two types of pores can be seen in this film, one of similar size to those in the films formed at voltages below 400 V (Fig. 4), while the second was much larger, likely due to the large and frequent sparks seen at high voltages and high currents. The number of small pores in any specific area in Fig. 5 is lower than in Fig. 4 and, in some areas, no pores are seen in the sample in Fig. 5. This was probably due to the partial sealing of small pores on the surface, caused by the application of voltages above 400 V. It should be noted that, in a parallel experiment employing the type B waveform, when anodization at 30 mA/cm^2 was stopped after 7 min without current decay, the oxide film also showed partial sealing of the small pores, similar to that seen in Fig. 5. Therefore, the formation of large pores and the partial sealing of smaller pores appears to be related primarily to the application of high voltages >400 V and not only to the existence of a current decay period.

When t_1 was extended to 10 min at 30 mA/cm^2 for another specimen, and the current was allowed to decay for 20 min to 25 mA/cm^2 (30 mA/cm^2 for 10, 20 min), the final voltage reached was 422 V. As the current was still quite high at this point, large and frequent sparks were observed. Fig. 6a shows the morphology of this film, which is quite different from that shown in Fig. 4, but more similar to that shown in Fig. 5. Again, there are two sizes of pores in the oxide film, small pores (0.5-2 μm) and larger ones (6-5

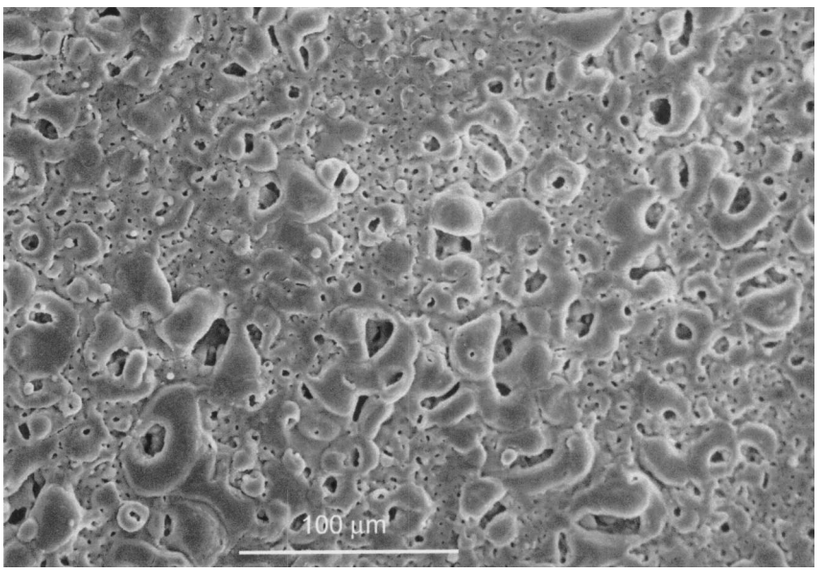

Figure 5. Top-view SEM image of the surface of WE43 alloy anodized at 30 mA/cm^2 for 7, 13 min.

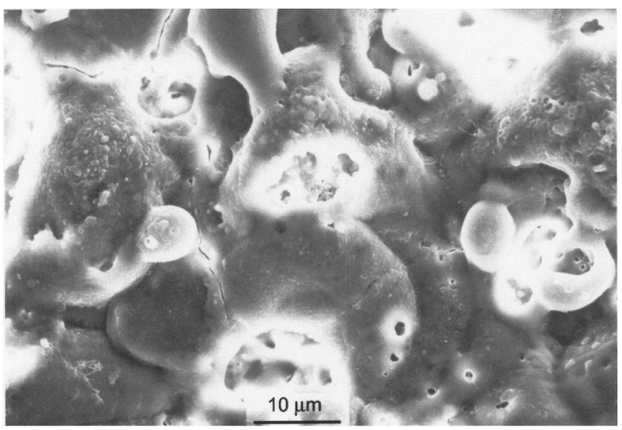

(a)

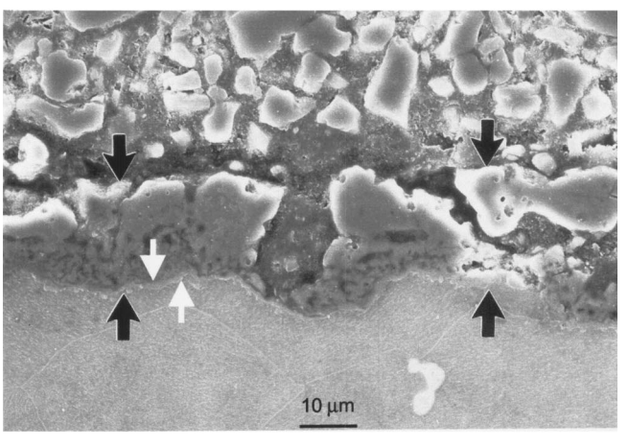

(b)

Figure 6. (a) SEM top-view morphology and (b) cross section of WE43 alloy anodized at 30 mA/cm^2 for 10, 20 min. Barrier layer is between white arrows.

μm). The number of small pores per unit area in Fig. 6a is much lower than in Fig. 4 and 5, demonstrating that some of the smaller pores may have fused at these high voltages (large sparks). However, the number of large pores is greater than in either Fig. 4 and 5. In addition, a few cracks were seen around the large pores in Fig. 6a. It appears that the high current/high voltage anodization of a specimen already coated with a thick oxide film, as in the experiments of Fig. 5 and 6, generated a large amount of heat, resulting in the fusing of the film and sealing of some of the smaller pores. At the same time, the large and frequent sparks seen on a thick oxide film under these conditions clearly resulted in the development of few, but very large, pores and the formation of cracks around the larger pores.

The cross-sectional image of the oxide film in Fig. 6a is shown in Fig. 6b. As in Fig. 4b, three separate layers can be seen clearly in the oxide film. The outer layer contained both small and large pores, with the diameter of the large pores increasing with increasing depth into the film. The intermediate layer contained pores that were distributed randomly and which did not penetrate through to the barrier layer. Compared with the pore size in this layer for films formed at 30 mA/cm^2 for 5 min, followed by current decay over 5 min (Fig. 4), anodization at higher voltages and higher current densities during the period of current decay appears to have lead to an increase in pore size.

As in Fig. 4, a compact barrier layer, which is *ca.* 1 μm thick, is seen sandwiched between the substrate and the porous oxide in Fig. 6b. The total thickness of the oxide film formed at 30 mA/cm^2 for 10 min, followed by a 20 min current decay period and under conditions such that the final total voltage and current were 422 V and 25 mA/cm^2, respectively, is almost twice that formed at 385 V, also at 30 mA/cm^2, as shown in Fig. 4. However, the barrier thickness increased by only *ca.* 20% when the final voltage increased from 385 to 422 V; this data is discussed in more detail in the following section.

Analysis of oxide film structure and thickness.—For a series of anodizations carried out at several constant current densities, the conditions were varied in order to determine the relationship between the waveform employed, the final anodizing potential, the current density, the film morphology, and the film thickness. It was observed that, with an increase in the anodizing voltage, larger and more frequent sparks, arising from the dielectric breakdown of the barrier film, were seen, correlating with the increase of the outer

Table II. Pore size, surface porosity, and oxide film thickness as a function of anodizing conditions at 10 mA/cm^2 using waveforms A and B.

Sample no.	Anodizing waveform and times	Final voltage, and current density (V, mA/cm^2)	Pore diameter (μm)	Porosity (percent of surface)	Porous layer thickness (μm)	Barrier oxide thickness (μm)
1	B, 5 min	286, 10	0.4-1.0	15	3.5	0.55
2	B, 10 min	318, 10	0.6-1.4	18	5.4	0.60
3	B, 15 min	354, 10	0.6-2.0	20	9.4	0.65
4	A, 5, 15 min	322, 0.5	0.6-1.4	20	6.4	0.6
5	A, 10, 50 min	372, 0.5	0.6-4.5	25	9.7	0.7

film pore size. This is in agreement with what has been reported for Mg oxide film growth using high dc voltage anodization methods in basic aluminate solutions.[16]

Table II shows the anodization conditions employed and the film properties obtained from the SEM analysis of a series of oxide films formed at WE43 at 10 mA/cm^2. Under all conditions at 10 mA/cm^2, only what we have classified as small pores, were formed, generally ranging from 0.5 to 2 μm in diam. For films formed using waveform B, the diameter of the pores on the surface, the surface porosity and the porous and barrier layer thickness all increased with increasing anodization time (and hence with increasing final voltages) at 10 mA/cm^2. When waveform A was employed, as shown in for samples 4 and 5 in Table II, the voltage continued to increase during the 15 min of current decay, *e.g.*, from 286 V after the initial 5 min at constant current (waveform B, sample 1) to 322 V (sample 4). During the period of current decay, both the porous and barrier layer thickness, as well as the pore diameter and surface porosity, increased further. That was probably caused by the increase in voltage when the current density decayed from 10 mA/cm^2 at 5 min to 0.5 mA/cm^2 after a total of 20 min.

For samples 2 (waveform B) *vs.* 5 (waveform A) in Table II, both anodized at 10 mA/cm^2, the voltage increased from 318 V after 10 min to 372 V after 50 additional min of current decay, to 0.5 mA/cm^2. With this increase of voltage, the average pore size and surface porosity both increased, along with the porous and barrier layer thickness. The increasing pore size with time of current decay may be correlated with the fewer, but larger, sparks seen at higher voltages.

Table III shows the analogous data to that in Table II but for the anodization of WE43 at the higher current density of 30 mA/cm^2, again using both waveforms A and B. It can be seen in Table III that, when using waveform B, a voltage of 360 V was required after 5 min (t_1), 396 V after 7 min (t_1), and 405 V after 10 min (t_1) to maintain a constant current density of 30 mA/cm^2. These voltages are all higher than required at 10 mA/cm^2, as expected. With the increase of anodizing time and voltage, both the porous and barrier layers became thicker. Notably, the porosity on the surface seen after 5 min of anodization, 28%, was much greater than the 15% seen at lower current densities (Table II) under otherwise similar conditions. Also, the small pores were larger in diameter for films formed at high *vs.* low current densities.

After 7 min at 30 mA/cm^2 (waveform B, samples 2 and 3 in Table III), a second type of pore, having a substantially larger diameter, was seen. Interestingly, once the larger pores developed, the number of small pores decreased, from occupying 28% of the surface area after 5 min to 16% after 10 min, while the number of large pores increased from 5 to 8% of the surface after 10 min. The total surface porosity remained relatively constant with anodization time using waveform B at 30 mA/cm^2.

As shown in Table III, when the anodization was carried out using waveform A at 30 mA/cm^2, the small pores were larger than for films formed for similar time periods by waveform B. However, as the larger pores formed after longer times of current decay (at higher voltages), the fraction of the surface covered by the smaller pores dropped, from 24% at 385 V to 12% at 408 V. Interestingly, the size of both the smaller and larger pores remained close to constant, independent of the final voltage when using waveform A.

It was observed during the anodization of WE43 that the frequency and size of the sparks decreased when a period of current decay (waveform A) was allowed. As was the case for the films formed at 10 mA/cm^2 in Table II, the voltage continued to increase during the period of current decay for the films formed at 30 mA/cm^2 in Table III. During the decay period, the porous and barrier film thickness both increased somewhat, and the number of large pores (porosity) also increased. However, the number of small pores decreased, while the diameter of both the small and large pores remained almost constant. The change in the number of small and large pores was likely correlated to the number of small and large sparks, respectively, seen during the decay period.

The relationship between the final total anodizing voltage (for both waveforms A and B) and the porous and barrier film thickness is shown in Fig. 7. In Fig. 7a, it can be seen that the relationship between the thickness of the porous film formed using either waveform A (squares) or B (circles) and the final voltage was linear. However, the line did not pass through the origin and the *x* axis

Table III. Pore size, surface porosity, and oxide film thickness as a function of anodizing conditions at 30 mA/cm^2 using waveforms A and B.

Sample no.	Anodizing waveform time	Final voltage, and current density (V, mA/cm^2)	Small and large pore diameter (μm)	Porosity, small and large pores (percent of surface)	Porous layer thickness (μm)	Barrier oxide thickness (μm)
1	B, 5 min	360, 30	0.4-2.6	28, 0	8.2	0.80
2	B, 7 min	396, 30	0.5-2, 10-15	20, 5	13.0	0.90
3	B, 10 min	405, 30	0.5-3, 8-15	16, 8	15.0	0.95
4	A, 5, 5 min	385, 10	0.8-3.6	24, 0	8.3	0.7
5	A, 7, 13 min	408, 4	0.6-4, 12-15	12, 0	15.0	0.95
6	A, 10, 20 min	422, 20	0.5-2, 6-15	5, 14	18.0	1.0

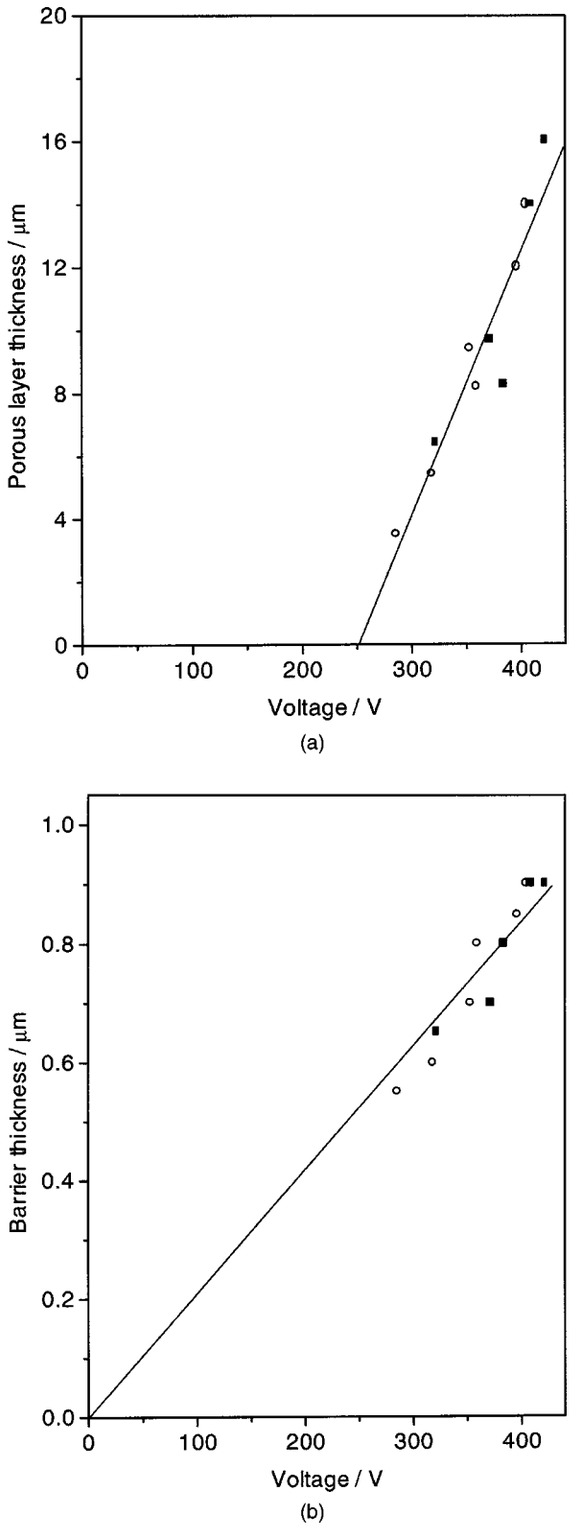

Figure 7. Oxide film thickness *vs.* final anodization voltage for films formed at WE43 at 10 and 30 mA/cm^2 in alkaline silicate solution. (a) Average total oxide film thickness and (b) barrier film thickness. (Squares) waveform A, (circles) waveform B.

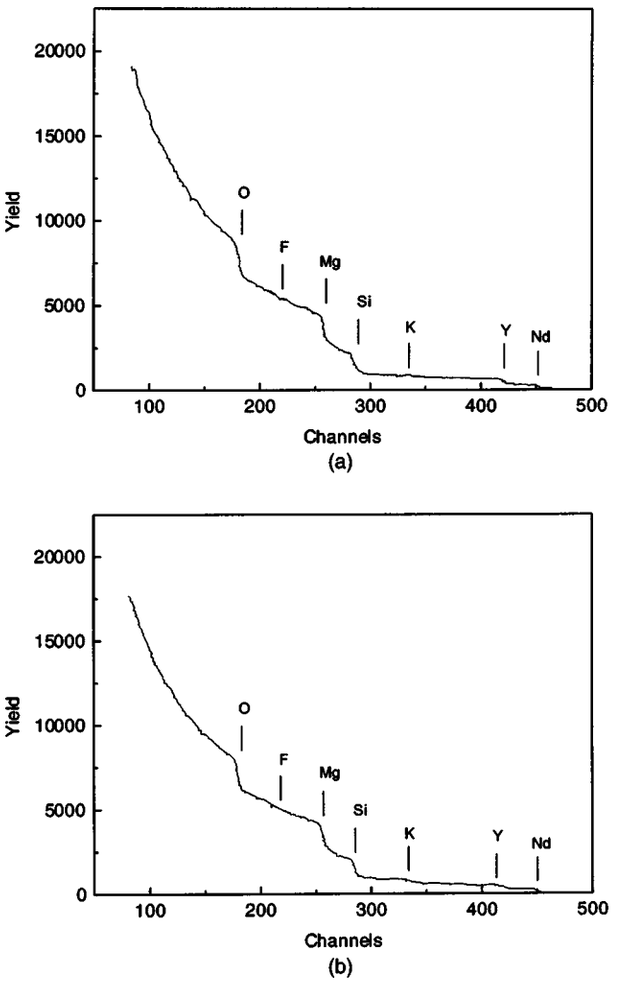

Figure 8. (Solid line) Experimental and (dashed line) simulated RBS spectra of oxide film formed at WE43 alloy by anodizing at 30 mA/cm^2 using (a) waveform A for 5, 35 min, and (b) waveform B for 5 min.

intercept is *ca.* 250 V (dc plus ac), suggesting that significant porous oxide film formation did not initiate until a voltage greater than this is applied. Then, the growth rate of the porous film was 70 nm/V, independent of the anodization current density and the waveform employed.

In Fig. 7b, a plot of only the barrier film thickness *vs.* the applied voltage also reveals a linear relationship. The slope yields an anodizing ratio of *ca.* 2.0 nm/V, independent of the current density and the type of waveform employed (waveform A squares, waveform B circles). The plot goes through the origin, demonstrating that the barrier film properties did not vary with applied voltage. This barrier film anodizing ratio was somewhat higher than that obtained for Al oxide films, formed by dc anodization in sulfuric acid or neutral solutions, *i.e.*, 1.5-1.7 nm/V,[26] but was close enough to these values to suggest that the barrier film was a poor ionic conductor and that it was thickened by a field-assisted process.[27,28]

Composition of oxide film formed at WE43.—The RBS spectra of two films, one formed at 30 mA/cm^2 (waveform B) for 5 min to 385 V and a second at 30 mA/cm^2 for 5, 35 min, finally reaching 390 V using waveform A, are shown in Fig. 8. The results show the presence of fluorine and silicon in both films. The incorporation of fluorine decreased with increasing final voltage and time using waveform A, in contrast to the silicon content. The concentration of magnesium remained the same in both films, independent of the formation conditions. As the final voltage and anodization time increased, and using waveform A, the concentration of potassium in

Table IV. Atomic concentration of elements in anodic oxide films at WE43.

	O	F	Mg	Si	K	Y	Nd
Film 1[a]	52.7	6.0	27.0	11.5	1.0	0.4	0.14
Film 2[a]	53.5	7.0	27.0	10.0	0.07	0.4	0.17
Substrate			99.5			0.3	0.11

[a] Films 1 and 2 were formed at 30 mA/cm^2 for 5, 35 min (waveform A) and for 5 min (waveform B), until a voltage of 390 and 385 V, respectively, was reached.

the oxide films increased as well. However, no sodium was detected in the oxide film using RBS, even though sodium silicate was used in the anodizing bath.

The composition of several oxide films formed at WE43 at 30 mA/cm^2 using both waveforms A and B is shown in Table IV. If Mg was present primarily as MgO and MgF_2, then the amount of remaining oxygen was consistent with the presence of SiO_2 in the film. The incorporation of silicon during anodization likely arose by the deposition of colloidal silica. This may form during anodization by the acidification of the solution near the alloy surface, according to Reactions 1 and 2

$$Mg + 2\ OH^- = Mg(OH)_2 + 2e^- \quad [1]$$

$$4OH^- = 2\ H_2O + \dot{O}_2 + 4e^- \quad [2]$$

The local acidity generated, in turn, results in the formation of silica, which is then incorporated into the oxide film

$$SiO_4{}^{4-} + 4H^+ = Si(OH)_4 \quad [3]$$

$$Si(OH)_4 + Si(OH)_4 + \ldots = (xSiO_2 \cdot yH_2O) \quad [4]$$

In any fluoride-containing solution, the formation of MgF_2 occurs, along with $Mg(OH)_2$.[29,30] In our case, the presence of fluorine in the oxide film was the result of the reaction between fluoride and Mg ions in the film. The increase in the local temperature due to sparking will also accelerate the growth rate of MgF_2. Y and Nd were also present in the oxide film, likely in combination with oxygen.

Based on the relative contents of each element in the oxide films in Table IV, the possible composition of the oxide film was $Mg(OH)_2$, MgO, MgF_2, SiO_2 and a small amount of K_2SiO_4, as well as Y and Nd oxide. The molar ratio of $Mg(OH)_2$, MgO, MgF_2, SiO_2 would then be 9.5:14:3.5:10 for the oxide film formed at a final voltage of 385 V (waveform B), and 8:16:3:11 for the film formed up to 390 V (waveform A). The increase in the MgO concentration and the decrease of $Mg(OH)_2$ (from the above analysis) with increasing final voltage and anodizing time demonstrated the transition of $Mg(OH)_2$ to MgO in the oxide film. As the barrier film was shown above to remain the same under all anodization conditions, likely as MgO, this suggests that the outer porous oxide film was initially $Mg(OH)_2$, which then decomposed to MgO. The increase in the SiO_2 concentration and the decrease in the MgF_2 concentration with increasing final anodization voltage and time suggests an increasing incorporation of colloidal silica under these conditions.

Correlation of corrosion resistance with oxide film properties.—The purpose of forming an oxide film on the WE43 alloy surface was to provide it with improved corrosion protection. As seen from the above results and from the literature,[15,16] a thick, but porous, oxide film, overlying an intact barrier oxide film, can be formed on the alloy by ac/dc anodization in an alkaline silicate based bath. The properties of both of these oxide layers have been shown above to depend strongly on the anodization conditions employed, *e.g.*, the waveform, anodizing current, final voltage, and anodization time.

Therefore, the corrosion resistance of the anodized WE43 specimens was determined in 0.86 M NaCl as a function of immersion time using the ac impedance technique. Figure 9 shows a typical set of impedance data, in both the Nyquist and Bode representations, for a type A (Fig. 9a) and a type B (Fig. 9b) film, both formed at 30 mA/cm^2, but differing by the period of current decay permitted for the type A film. The impedance data shown in Fig. 9a and b were collected at the OCP after 24 h of immersion in 0.86 M NaCl. These were then best-fitted using an equivalent circuit (see insert of Fig. 9) consisting of two (R-CPE) components in series with the solution resistance, R_s, between the WE43 electrode and the reference electrode. Here, R is a film or reaction resistance and a CPE is a constant phase element, which reflects the dispersion of a capacitive element (*e.g.*, the film dielectric capacitance) around a central value.[31,32]

Both the experimental data and the calculated overlays, based on a best fit to this equivalent circuit, are shown in Fig. 9. The corrosion resistance of the ac/dc anodized WE43 could then be determined from the sum of R_1 and R_2, found to be similar to the resistance obtained if a single time constant equivalent circuit was used, as R_1 and R_2 in the two-time equivalent circuit for impedance data fitting likely represent the resistance of inner barrier and outer porous layer, respectively.[33] Figure 10 shows the corrosion resistance ($R_1 + R_2$) as a function of immersion time for a series of oxide films formed at 30 mA/cm^2 using the type B waveform for 5 and 10 min, and using the type A waveform, as follows: 5, 5 min; 7, 13 min; and 10, 20 min. The sample number, the thickness of both the overlying porous and the inner barrier oxide film, the average pore diameter, and the surface porosity of each film are given in Table III.

Figure 10 shows that the corrosion resistance changed with time, and that three regimes can be identified. In the first 3 h, the corrosion resistance decreased very rapidly with time. In the next approximately 10 h, the corrosion resistance increased, reaching a peak, and then the resistance dropped again in the third phase, until the oxide film failed and pitting was seen (or the corrosion resistance suddenly decreased to $<$10,000 Ω). A more rigorous analysis of the mechanism of film breakdown, in relation to these three time periods, will be presented in a later paper.[33]

As can be seen from Fig. 10, the general trend is that the shorter anodizing times led to earlier failure, as expected. The poorest film (sample 1) was formed at 30 mA/cm^2 for only 5 min, although the additional period of time of current decay (5 min) for sample 4 clearly provided additional benefits. Table III shows that the latter film had a thicker porous and barrier film, and a lower surface porosity. The two films formed on samples 3 and 5 in Table III, *i.e.*, in 10 min (waveform B) and 7, 3 min (waveform A), respectively, exhibit the highest corrosion resistance after 60 h of immersion in the NaCl solution. In the first 20 h, the film formed at sample 5 in 7, 13 min (waveform A) has a similar corrosion resistance to the film formed at sample 3, *i.e.*, formed in 10 min (waveform B). However, the former has a much higher resistance than the latter at immersion times between 20 and 60 h, even though both films experienced the same final anodization voltage. Therefore, the films formed using waveform A did exhibit a higher corrosion resistance, overall. Notably, both of these films, formed to a very similar final voltage, had a similar porous and barrier film thickness and similar pore diameters (Table III). The difference in the corrosion resistance between these two films was probably caused by the small difference in the total number of both the small and large pores (surface porosity), as shown in Table III. Sample 5 had fewer small pores but a greater number of large pores than did sample 3. However, the total porosity of sample 5 was slightly less than that of sample 3.

It can also be seen in Fig. 10 that the oxide film formed at 30 mA/cm^2 in 10, 20 min (sample 6 in Table III) had a lower corrosion resistance than that formed at 30 mA/cm^2 for 7, 13 min (sample 5, Table III), even though the former film had a thicker porous and barrier film than the latter. As shown in Table III, the total surface porosity of sample 6 was lower than that of sample 5, due to the significant decrease in the number of small pores. However, a greater number of large pores were seen for sample 6, from 10% of

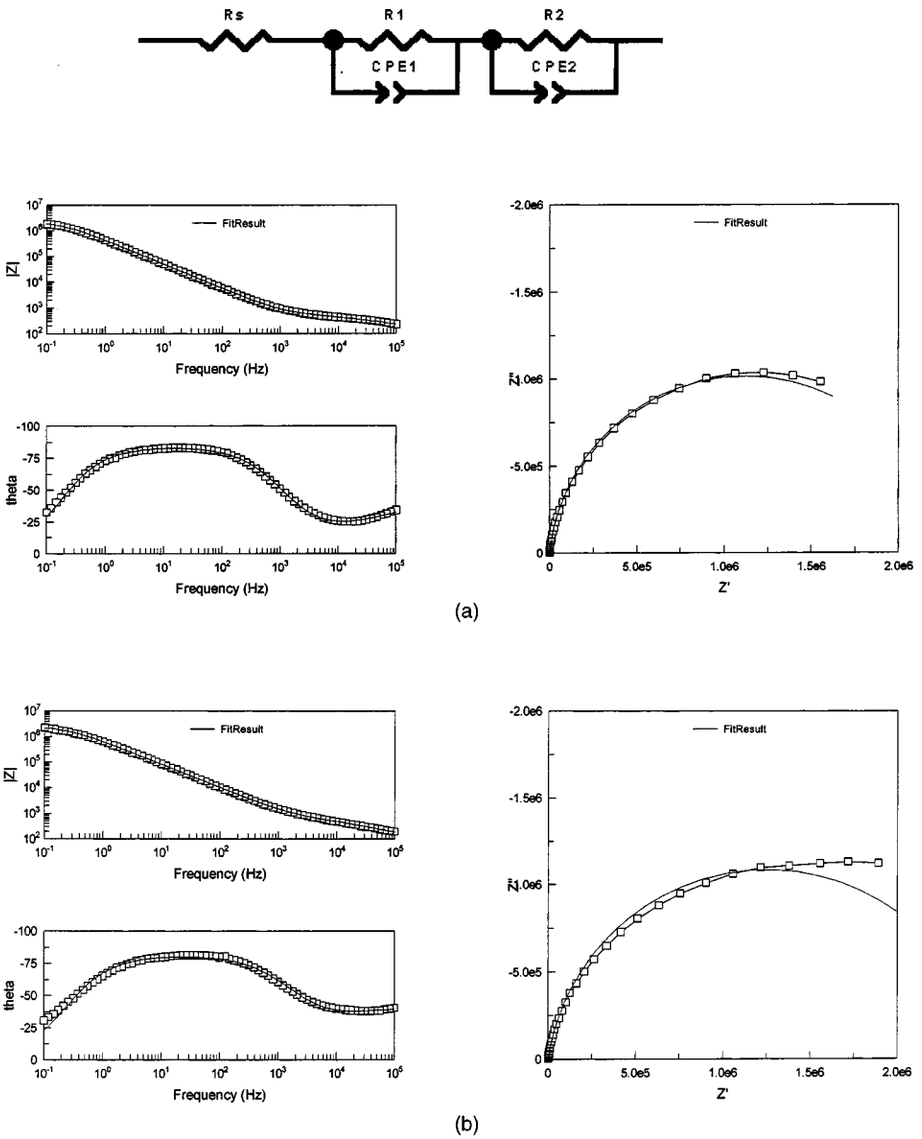

Figure 9. (Solid line) Experimental and (dashed line) theoretical Nyquist and Bode impedance plots for anodized WE43 samples in 0.86 M NaCl solution after 24 h of immersion. (a) oxide film was formed at 30 mA/cm^2 for 7, 13 min; (b) oxide film was formed at 30 mA/cm^2 for 10 min. The equivalent circuit employed for impedance fitting is also shown in the figure.

the surface for sample 5 to 14% for sample 6. The SEM image of sample 6 (Fig. 6a) also shows the presence of a few cracks around the large pores, both factors likely leading to its earlier failure during corrosion testing.

Therefore, the improvement in the corrosion resistance- which could be achieved by increasing the oxide film thickness by using higher anodization voltages- was limited by the fact that large pores, with associated film cracking, also developed, likely due to the generation of large and frequent sparks under these conditions. Therefore, the correlation between the corrosion resistance and the total oxide film thickness, including the barrier film thickness, was complicated when large pores (above 6 μm in diam) were formed, and when the smaller pores were partially sealed during anodization. Further, oxide films formed at lower voltages, *i.e.*, those which did not contain any of the larger pores and which had a barrier film thickness less than 0.90 μm, exhibited a corrosion resistance which seemed to be primarily proportional to the barrier film thickness.

Conclusions

Two types of waveforms were employed in the ac/dc anodization of the WE43 alloy in an alkaline silicate solution. In both cases, an anodizing voltage of *ca.* 190 V was applied initially. In waveform A, the desired constant current density was then maintained for a period of time, followed by a period of time of decreasing current, while in waveform B, the current density was kept constant throughout the anodization process. The oxide films thus formed were all composed of an underlying barrier layer and a thick porous oxide film, the latter sometimes seen to be composed of two layers. The outermost of these two layers appeared to contain larger pores than the intermediate layer, and the pores were interconnected, but did not penetrate the inner barrier film.

For either waveform employed, at low anodization current densities (*e.g.*, 10 mA/cm^2), only small pores (0.5 to 4 μm in diam) were formed, while at 30 mA/cm^2, both small and large (5-15 μm diam) pores were observed, likely related to the size of the sparks seen visually. Longer times of anodization at 10 mA/cm^2 caused the small pores to become somewhat larger in diameter and in number. At 30 mA/cm^2, while the small pores also became a little larger with longer anodization times, they decreased in number as they were sealed, especially above 400 V, being replaced by the larger pores, which increased in number. However, in both cases, the higher voltages reached at longer times also caused both the barrier and overlying porous films to thicken substantially and cracks to develop around the large pores.

The thickness of the barrier film depended linearly on the final voltage employed, yielding an anodization ratio of 2 nm/V. The

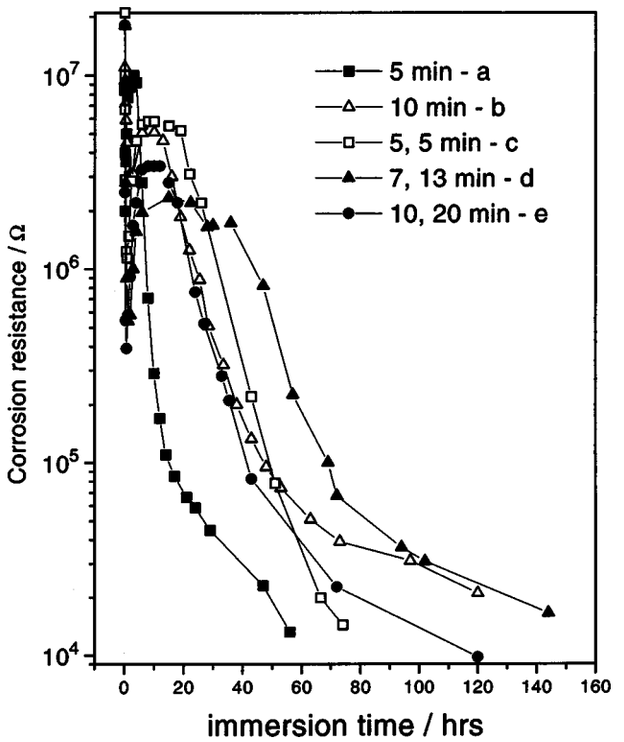

Figure 10. Corrosion resistance of anodized WE43 samples as a function of immersion time in 0.86 M NaCl solution. The WE43 samples were anodized as follows: at (a) 30 mA/cm^2 for 5 min, (b), 10 min, (c) 5, 5 min, (d) 7, 13 min, and (e) 10, 20 min.

barrier film appeared to have the same properties under all anodization conditions employed. In contrast, the porous film thickened at a rate of 70 nm/V, but only after a voltage above 240 V has been reached, independent of the current density and the type of waveform employed. The oxide film was composed of MgO, $Mg(OH)_2$, MgF_2, and SiO_2, with their molar ratios depending on the final voltage and total anodization time. An increase in the final anodization voltage and time led to an increase in the MgO and SiO_2 and a decrease in the $Mg(OH)_2$ and MgF_2 content of the films.

The corrosion resistance of these anodized specimens was generally seen to be highest for films formed at higher voltages (longer times, higher currents). This demonstrates that the increasing thickness of both the barrier and porous layers achieved outweighed the increase in the total pore area in providing corrosion protection. However, the improvement in the corrosion resistance by increasing the oxide film thickness became limited at voltages $>$ *ca.* 410 V due to the increasing number of large pores and cracks which developed under those conditions. Oxide films of the same thickness, formed at WE43 using waveform A, did exhibit a slightly higher corrosion resistance overall, likely due to the fewer number of small pores present than for films formed using waveform B.

Acknowledgments

The authors gratefully acknowledge Honeywell Engines Systems and Services for financial support, the South Bend Materials Technology Center for the SEM examination of samples, and Charles Evans & Associates for the RBS analyses.

The University of Calgary assisted in meeting the publication costs of this article.

References

1. P. Greenfield, *Magnesium, M&B Monography ME/11*, Mills & Boon Limited, London (1972).
2. P. Lyon, J. F. King, and G. A. Fowler, *J. Eng. Gas Turbines Power*, **115**, 193 (1993).
3. G. A. Fowler, J. F. King and P. Lyon, *Corrosion Resistant Magnesium Alloys*, Magnesium Electron Ltd. Swinton, Manchester, England (1990).
4. J.-M. Arlhac and J-C. Chaize, Personal communication (1996).
5. MEL Data Sheet 467A, Electron WE43, August (1997).
6. J. H. Waibel, *Metals Handbook*, Desk Edition, Chap. 8, p. 1, ASM International, Metals Park, OH (1985).
7. R. G. Rateick, Jr., *Introduction to Cast Magnesium Alloy Technology*, ASCA-861-22218R, Honeywell, South Bend, IN (1993).
8. B. Burako and J. Joesten, in *Proceedings of the 49th Annual World Conference of the International Magnesium Association in Chicago*, Vol. 2, p. 87 (1992).
9. B. Geary, in *Proceedings of the International Conference on Advanced Aluminum and Magnesium Alloys*, American Society for Metals, p. 773 (1990).
10. H. A. Evangelides, U.S. Pat. 2,723,952 (1955).
11. The Dow Chemical Company, G.B. Pat. 762,195 (1956).
12. M. Weiner, *Met. Finish.*, **93**, 65 (1995).
13. A. J. Zozulin and D. E. Bartak, *Met. Finish.*, **92**, 39 (1994).
14. L. L. Gruss and W. McNeil, *Electrochem. Technol.*, **1**, 283 (1963).
15. F. A. Bonilla, A. Berkani, Y. Liu, P. Skeldon, G. E. Thompson, H. Habazaki, K. Shimizu, C. John, and K. Stevens, *J. Electrochem. Soc.*, **149**, B4 (2002).
16. O. Khaselev, D. Weiss, and J. Yahalom, *J. Electrochem. Soc.*, **146**, 1757 (1999).
17. O. Khaselev and J. Yahalom, *J. Electrochem. Soc.*, **145**, 190 (1998).
18. S. Ono, K. Asami, T. Osaka, and N. Masuko, *J. Electrochem. Soc.*, **143**, L62 (1996).
19. R. G. Raiteck, Jr., S. J., Xia, and V. I. Birss, in *Magnesium Technology*, H. I. Kaplan, Editor, p. 289, The Minerals, Metals, and Materials Society, Warrendale, PA (2002).
20. D. E. Bartak, B. E. Lemieux, and E. R. Woolsey, U.S. Pat. 5,266,412 (1993).
21. E. L. Schmeling, B. Roschenbleck, and M. H. Weidemann, U.S. Pat. 4,978,432 (1990).
22. V. I. Birss and R. Yue, Canadian Pat. 2233339 (1998).
23. T. F. Barton and C. B. Johnson, *Met. Finish.*, **29**, 138 (1995).
24. G. Patermarakis, P. Lenas, C. Karavassilis, and G. Papayiannis, *Electrochim. Acta*, **36**, 709 (1991).
25. G. E. Thompson and G. C. Wood, *Treatise on Materials Science and Technology*, J. C. Scully, Editor, Vol. 23, Academic Press, London (1983).
26. S. Wernik, R. Pinner, and P. G. Sheasby, *The Surface Treatment and Finishing of Al and Its Alloys*, 5th ed. Vol. 1, ASM International, Metals Park, OH (1987).
27. P. H. G. Draper, *Corros. Sci.*, **7**, 91 (1967).
28. D. J. Stirland and R. W. Bicknell, *J. Electrochem. Soc.*, **106**, 481 (1959).
29. J. H. Nordlien, S. Ono, and N. Masuko, *J. Electrochem. Soc.*, **142**, 3320 (1995).
30. S. Yamaguchi, *J. Appl. Phys.*, **24**, 1437 (1954).
31. M. Leibig and T. Halsey, *Electrochim. Acta*, **38**, 1985 (1993).
32. R. D. Armstrong and R. A. Burnham, *J. Electroanal. Chem. Interfacial Electrochem.*, **257**, 72 (1978).
33. S. J. Xia, R. Rateick, and V. I. Birss, *J. Electrochem. Soc.*, To be published.